From MRI to anatomical simulation of the hip joint

Lazhari Assassi, Caecilia Charbonnier, Jérôme Schmid,

Pascal Volino, Nadia Magnenat-Thalmann

MIRALab - University of Geneva, Geneva, Switzerland

email: lazhari.assassi@miralab.unige.ch

Abstract

This paper describes a methodology for the simulation of musculoskeletal disorders. Our clinical study is related to osteoarthritis of the hip, a pathogenesis possibly due to impingements. These bone collisions lead to abnormal joint mechanics which is characterized by contact pressure and stress distribution upon the joint cartilages. The proposed methodology combines different approaches from modeling to simulation. The simulation is based on patient-specific anatomical models, where acquisition modalities are non invasive and flexible. Based on static MRI (Magnetic Resonance Imaging) data, a discrete deformable models method is used for modeling the organs of the musculoskeletal system. Femoroacetabular movements are estimated using an optical motion capture system and are validated by a dynamic MRI analysis. To achieve accurate deformation, techniques to generate volumetric meshes are developed based

on the medial axis information. Finally, a computationally-efficient fast functional joint model is used to simulate the mechanical behavior of the soft tissues. The goal of such a simulation is to allow the investigation of the relevant contact and cartilage deformation under movement, which can be useful for diagnosis, pre- or post- operative planning and training. This will benefit further developments in surgical techniques and minimalized invasive procedures.

Keywords: Anatomical modeling, physical-based simulation, hip motion analysis, computer simulation, hip osteoarthritis.

Introduction

Musculoskeletal disorders are common causes of different pathologies and physical disability, affecting many people across the world. Among these pathologies, osteoarthritis (OA) also known as degenerative joint disease is the most common and frequent form of arthritis. This pathogenesis is characterized by the breakdown of the joint's cartilages. Indeed, bones rub against each other, causing stiffness, pain and loss of movement at the joint. These bone collisions are generally referred to as impingements. However, the causes are still not completely known and need, hence, to be further evaluated. Previous studies have shown that the causes are related to several factors such as genetics, age, obesity, infections, etc. Moreover, ongoing research is investigating the statistical correlation between extreme movements and arthritis [1].

Our clinical focus is to study the causes of the hip OA [2]. The diagnosis of this pathology is usually based on medical images analysis and examination of the patient. Clinical motion patterns (flexion/ extension, add/ abduction, internal/ external rotation) are also used to diagnose impingements. Such practical methods strictly depend on the patient's feedback. Therefore, the diagnosis may not be accurate [3]. Thus, estimating the contact and stress distribution is critical for the understanding of the pathology, as well as for the pre-operative planning and the post-operative rehabilitation. To this end, computer graphics offer a wide range of possibilities to process medical data and extract relevant information.

The purpose of this study is to devise a methodology for the physical-based simulation of

the hip joint. Figure 1 provides a schematic overview of the whole process. First, from non-invasive and flexible data acquisitions patient-specific models of bones and soft tissues are reconstructed. Second, a marker-based system is used for the estimation of the hip movements. The optical motion capture is the standard for measuring and analyzing human motion in both the clinical and non-clinical environment. Third, physical-based simulations require volumetric models of anatomical structures to reproduce the actual biomechanical behavior. To generate these volumes, a method based on medial axis information is considered. Finally, a fast functional joint model is used to achieve accurate and realistic soft tissues deformation.

This paper is organized as follows: the next section is dedicated to the existing work and broadly reviews the field. Advantages and limitations of existing methods are discussed. Then, the methodological steps of our proposed methods and experimental results are presented. We conclude with our future work and perspectives.

Related work

The musculoskeletal system is composed of different complex and heterogeneous elements. It provides form, support, stability, protection and locomotion. Modeling this system remains a big challenge due to its complexity of geometry, mechanical behavior and interactions. Consequently, the study of the human body was divided into different disciplines. Despite the interdependencies, the models developed in the various domains focused on one

specific aspect. Nowadays, creating a complete and accurate human model is a difficult task. One interesting example of such attempt is the 3D Anatomical Human project [4] involving a pluri-disciplinary network in order to exchange and combine knowledge from different expertise domains. In the same context, the Co-Me (Computer Aided and Image Guided Medical Interventions) project [1] connects clinics and engineering sites in Switzerland to develop applied technologies for specific clinical applications.

Our developments are part of these two projects with a specific focus on the interactive clinical visualization of the hip joint examination. This topic was the subject of many researches. Indeed, simulations based on 3D models extracted from MRI and CT datasets were proposed (e.g., surgical planning [5, 6] and range of motion estimation [7]). The analysis of the stress and contact distribution in the acetabulum region also contributed to the understanding of the hip biomechanics (e.g., Mass-Spring [8, 9] and Finite-Element methods (FEM) [10, 11]).

The goal of our study is to produce accurate and realistic simulations of the hip joint. This will allow the investigation of the relevant contact and cartilage deformation under movement. To this aim, several aspects from modeling to simulation should be considered. We first provide a literature review of the previous techniques, our methodology is then described in the next section.

Anatomical modeling

Anatomical modeling addresses the problem of image segmentation. It consists in extracting anatomical structures from medical data acquisitions such as MRI. This modality is appropriate for the simultaneous examination of soft and bony tissues. But clinical MRI datasets present large amount of textural information, noise, and low resolution artifacts. Moreover, the musculoskeletal system is very complex and large anatomical variations exist among individuals. As a result, no method has proven to be generic, automatic and robust. In many cases, anatomical modeling is interactive and time consuming [12, 13], or not individualized [14]. Direct segmentation involves a detection step where regions are identified in images and a classification step where regions are combined to create new ones. But for musculoskeletal system segmentation, direct segmentation is noise-sensitive, not robust and quite inaccurate. The use of prior knowledge can considerably improve the segmentation by enforcing constraints. For instance, prior information can be defined as (valid) shape variations across population [15, 16], topological constraints (e.g., attachments [17]) or organ smoothness. Furthermore, statistical priors can be naturally coupled with Bayesian approaches that formulate the segmentation as a Maximum A Posteriori problem [16].

Computer graphics techniques can be used to devise more adapted segmentation methods. Deformable models of Terzopoulos et al., originally presented in a computer graphics context, gave birth to novel approaches in medical imaging analysis [18]. Deformable models can adopt various kind of representations: deformable contours (snakes) [19], paramet-

ric [20], implicit (e.g., level-set [16]) and discrete [21, 17]. In particular, physical-based deformable models [22, 23] were successfully applied to segmentation [17, 24]. Recent advances in the computational power of graphics processing units (GPUs) resulted in a new generation of very fast GPU-based segmentation methods [25, 26]. These methods are interactive since the segmentation evolution is observed and controlled during the computation. However, GPU architecture imposes some constraints (sometimes too restrictive), like the choice of data structures and the type of numerical integration schemes [27].

Volumetric meshing

Nowadays, there is a growing use of the physical-based models in the computer graphics field to achieve more accurate simulations. Most existing models are surface-based, however, these approaches are unsatisfactory for applications where the object's internal representation is essential (e.g. models cutting simulation).

Unstructured meshing methods for 3D objects based on hexahedra and tetrahedra elements were used in many research areas. Three main techniques were proposed for tetrahedral mesh generation. The Octree-based method subdivides recursively the bounding box enclosing the object in regular sub-cells until the desired resolution is obtained [28]. In addition to a large number of surface intersection calculations, the elements generated near the boundary are of poor quality. Molino et al. [29] approach allows proper cells connections and improves approximation of the initial mesh through optimization routines. The

Advanced front approach starts from the object boundary and moves towards the empty space within the object. The difficulty in this process is to calculate the ideal node location where the node will be connected. According to the sizing function and the quality of the element, different methods were developed [30, 31]. The Delaunay approach is based on the Delaunay criterion (no nodes can be inside the circumsphere of any tetrahedron). This criterion offers a rule for connecting a set of 3D points. However, two main problems may occur in the constructed mesh: it does not fit the original mesh and some of its tetrahedra are of poor quality (i.e. slivers). Different Delaunay refinement methods were studied for improving the resulting degenerated elements [32, 33]. The Constrained Delaunay Triangulation (CDT) technique enforces boundary conformity [34]. Optimization methods can be applied to improve the mesh quality by moving nodes, swapping edges/ faces between adjacent tetrahedra and inserting/ deleting elements [35, 36].

Additional hexahedral-based techniques were proposed. The grid-based method [37] starts by filling the internal object with regular hexahedra. Then, the open space between the external constructed mesh and the object boundary is meshed. The Plastering method is similar to the advancing front approach with hexahedra elements [38]. The Whisker weaving algorithm [39] first constructs the spatial twist continuum (STC: dual of the hexahedra mesh) [40]. The medial surface method [41] decomposes the volume in a set of medial surfaces. The STC and the medial surfaces are both utilized to fill the volume with hexahedra.

Other researches focused on 3D image-based meshing techniques. The developed methods combine segmentation and mesh construction. For example, tetrahedral meshes were

constructed using slice data [42, 43] and hexahedral meshes were generated using Medial representation (M-Rep) [44].

As mentioned in this overview, the meshing methods require successive steps and post-processing routines to improve the constructed mesh. The input model and the application play a fundamental role in the adoption of the technique. Moreover, the hexahedral meshes offer important computational advantages, however, tetrahedral meshing techniques are faster, more robust and capable to handle complex geometry.

Human motion analysis

Estimating joint kinematics in the 3D space requires the determination of the instantaneous position and orientation of the bones under investigation. To this end, one of the most common methods to measure joint movement is to track the motion of clusters of three or more reflective markers affixed to the skin of the bone segment. In computer graphics, these systems are conventionally used for the animation of virtual characters, but can also be helpful for medical applications. However, the internal bone remains inaccessible and the resulting estimations are embedded with soft tissue artifacts (STA) leading to subjective and misleading diagnosis. Displacements of individual markers with respect to the underlying bone of more than 20 mm are observed [45] and the STA associated with the thigh is greater than any lower limb segment. A robust way to assess joint kinematics is the use of intracortical pins [46], external fixators [45], percutaneous trackers [47] and fluoroscopy [48].

This avoids soft tissues behavior problems but these approaches are strongly invasive and impede natural motion patterns. Mathematical methods to minimize the effect of STA have been implemented. Cappello et al. [49] devised a double calibration method to reduce errors associated to non-rigid markers' movements. Luchetti et al. [50] used ad-hoc movements and quantified the skin movement throughout the range of motion. They determined the correlation between skin markers artifact trajectories and flexion-extension angles. This approach is however limited since it assumes that skin motion during the artifact assessment movements is the same as during the dynamic activities. Alexander and Andriacchi [51] developed a Point Cluster Technique (PCT) by using a cluster of large number of markers and an optimal weighting to lessen the effect of STA. A recent study [52] has shown that the PCT is unstable and it does not perform better than traditional bone pose estimators. Techniques that iteratively and globally optimize joint center locations and segment orientations are applied [53]. Rather than estimating skeletal pose of each segment individually, these techniques model the articulations as ball and socket joints and use a multi-link musculoskeletal model with joint constraints. Considering the physiological motion of the joint into the overall estimation of segment poses is really appropriate, however the assumption of ball and socket joints simplifies the joints structures. Therefore, our approach is based on a global optimization, but in contrast to previous works we propose in this study to account for the patient's anatomy (3D meshes) and kinematics (hip joint center). The use of subject-specific 3D models reconstructed from MR images results in the fact that the joint is no more considered as a perfect ball and socket.

Physical simulation

Physical simulation computes the deformation of the tetrahedral discretization of the mechanical objects. Most simulation techniques express the mechanical behavior of the material as strain-stress relationships formulated according to the internal forces and deformations of the tetrahedral element. The resulting numerical system is then integrated with adequate numerical methods for obtaining either the static equilibrium state (relaxation) or the dynamic evolution of the system along time (motion). The Finite-Element method closely follows this scheme.

Finite-Element methods [54] proceed in several steps. First, a deformation tensor is expressed at each point inside the elements, based on the shape functions associated with the nodes. When linear shape functions are used, the elements are called first degree, otherwise they are called higher degree. First-degree elements are simple and offer good performance, as their degree of freedom are typically only represented by the vertex positions of the mesh representing the object. Thus, material strains and stresses, which are typically considered uniform over the element, can easily be computed. With the additional simplification which condenses the mass of the material on these mesh vertices (mass lumping), these representations become equivalent to particle systems, which represent the mechanical system as a set of masses which interact through forces computed from their relative positions. Higher-degree elements are appropriate when higher degree of continuity is required in the approximation of mechanical properties between the elements, but lead to more complicated

formulations.

Numerous authors have attempted to speed up the computation times required for Finite-Elements. Pre-inverting the linear system matrix may speed up the computation [55, 56], but is only practical when the mechanical system is small enough. Condensing the dynamics on the boundary of a closed volume can reduce the number of unknowns to solve at each time step. These precomputations are possible when the force-displacement relation is linear, which requires both geometrical and material linearity. Large deformations are usually handled in two different ways. The most straightforward is to use Green-Lagrange's nonlinear strain measurement, while keeping material linearity. This is called the St-Venant-Kirchhoff model, mainly used in volume simulation [57, 58, 59, 60].

The force-displacement behavior of St-Venant-Kirchhoff models is less "intuitive", through the nonlinearity of their strain and stress tensors. Hence, their strain is not proportional to the deformation of the material, and the exerted force is not proportional to the stress. Actually, with strain-stress proportionality, the tensile force-deformation curve of such a material is cubic. However, their mathematical definition is indeed the most mathematically natural way of expressing strain and stress, and indeed the simplest, despite the nonlinearity.

The major drawback of this model is that it is not robust under large compression, since it is prone to collapse [57]. Recently, a new approach has been proposed, where the strain tensor is factored as the product of a pure rotation with Cauchy's linear strain tensor aligned along the strain eigendirections [61, 62, 63, 64]. This corotational approach has become very popular, as it combines the computational simplicity of using the linear Cauchy tensor

with large deformations. This approach has been successfully used in cloth simulation [65]. However, this approach requires additional computations for finding the eigendirections of the strain tensor and managing the rotations accordingly (particularly when dealing with anisotropic materials such as cloth). Furthermore, the effects of these directional changes are not taken into account in the Jacobian, which is therefore not perfectly accurate. Therefore, this method is mainly suited for simulating perfectly linear isotropic material with large deformations.

Methodology

Segmentation and anatomical reconstruction

A high accuracy is mandatory in medical segmentation. For a correct diagnosis, it is indeed essential to capture patient-specific details. Since an ubiquitous trade-off between accuracy and speed exists in any segmentation technique, some approaches thus yield high computation time. Not mentioning the tedious tuning of these slow methods, a direct integration in clinical sites is highly compromised. This is problematic because relevant clinical input is needed for the validation and the adjustment of segmentation techniques. We present a method that avoids the shortcomings of slow methods while preserving a good accuracy with clinical images. The method particularly exploits some computer graphics techniques from the physical-based simulations literature [66, 23, 67].

The structures of the generic models to be segmented (bones, muscles, ligaments and cartilages) are created only once with an interactive segmentation method. These meshes are computed at different resolutions to be used in our multilevel scheme (more details follow). A 2-simplex meshes description [21] (dual to triangle meshes) is used for models. In case of 2-simplex meshes, three affine-invariant parameters uniquely define vertex positions from their three neighbors. These parameters are denoted as simplex parameters. The segmentation strategy then consists in deforming the generic models until they match the corresponding structures. Starting from a manual initialization based on landmarks' placement and Thin-Plate Splines interpolation, the deformable meshes evolve under the influence of internal and external forces. Model vertices are in fact considered as punctual masses evolving under the Newtonian law of motion. The Newton equation relates forces to particle position and velocity. The resulting differential equations system is time discretized and solved by a stable implicit integration scheme [23].

The overall strategy consists in first segmenting the bones, then the cartilages and finally the soft tissues (ligaments and muscles). During the segmentation, higher mesh resolutions are used in combination with lower resolutions. We exploit a forces propagation scheme between different resolutions, which linearly combines lower with higher resolution forces. This approach confers robustness and accuracy. Additionally, non-penetration constraints are implemented with collision handling [68] and response [67] techniques. For shape regularization, we use a smoothing force that penalizes strong irregularities and forces that impose shape constraints. Shape constraints rely first on a statistical analysis of shapes

variation that follows an approach similar to Cootes' et al. PDMs [15]. Moreover, hard constraints are simply enforced on shapes by predefining their simplex parameters [21, 17]. We also exploit the medial axis representation of soft shapes like muscles to create internal constraints. In soft tissue segmentation, topological constraints are also accounted by modeling bone-tendon attachments. The soft tissue vertices are then constrained using mass modification [66] to realize the desired constraints. Eventually, intensity profiles extracted along mesh normals are registered with generic profiles from a reference segmentation to produce external forces. The external force field is then regularized using a local smoothing and global regularization based on the closest affine transformation.

We validate our methods for the hip joint and the thigh (21 muscles, 4 bones, 3 cartilages and 3 ligaments) on 4 datasets. An appropriate MRI protocol was defined in close collaboration with departments of radiology and orthopaedics. The automatic segmentation is compared with reference manual segmentations performed by experts. The results depict an accurate (error=1.5 mm) and fast (computation time=15 min) method. Figure 2 illustrates some segmentation results with different reconstructed models examples. The interested reader can refer to [17, 69] for further details.

Volumetric modeling

Classical meshing techniques cannot always generate accurate tetrahedral meshes. Generally, the generated mesh presents reconstruction defaults such as errors in thin parts, low

quality elements and inconformity with the initial surface boundary. Indeed, these techniques do not account for the model thickness during meshing. Thus, we propose a method that generates tetrahedral meshes where the resolution is distributed according to the thickness of the model. Medial Axis Transform [70] consists in finding the maximum balls inscribed in the object which are defined by their center and radius. Several techniques based on Voronoi diagrams, distance maps, and thinning have been proposed to approximate the medial axis (MA). Despite the fact that both topology and boundary locations of the object are well-defined, the generated MA are very sensitive to the surface smoothness (perturbations on surface create excessive branchings in MA). To overcome this problem, pruning approaches simplify the MA by suppressing redundant parts. However, the MA is then no more homotopy equivalent to the model. In the context of object segmentation, Pizer et al. [71] proposed an efficient M-Rep-based approach. The medial axis is then constructed by fitting a simple deformable model to the middle of the object. This approach provides a good representation of objects by their medial sheet.

Based on the assumption that muscles, ligaments and cartilages do not have branching in their medial sheet representation, we adopt this approach to compute their medial axis. MA implied boundaries will fit the object surface and will be used to construct the corresponding tetrahedral meshes. In a first step, we construct a uniform rectangular grid (denoted as medial grid) composed of nodes with radius R_j and position Q_j. This grid will be deformed to approximate the MA as follows (see Figure 3A). In a first step, the node parameters R_j and Q_j are iteratively updated by using forces f_j based on radial and smoothing constraints.

The purpose of radial forces is to minimize the distance between the model and the reconstructed surface from the medial axis. Smoothing forces ensure grid cell regularity and resizing according to node parameters. Under the influence of these forces, the medial grid progressively converges to the medial axis.

In a second step, each medial axis node Q_j is projected on the model with respect to both sides of the medial axis. Then, grid cells are extruded by subdividing equally the distances $Q_jQ_{j\perp}$ and by inserting new nodes (see Figure 3B). Moreover, for rim atoms, projected nodes are added to reproduce the curvature around the crest of the object. Eventually, all nodes are combined to create tetrahedra. Special care is taken in defining their adjacency. Figure 4 and Table 1 show the results achieved by the proposed technique compared to two reference methods [72, 36] based on Delaunay approach. The main indicators of tetrahedralization are the number and the quality of tetrahedra, and the accuracy of the volumetric mesh envelop. To assess tetrahedra quality, we use the dihedral angle and the aspect ratio. The aspect ratio histograms of the results are presented in Figure 4. The proposed method offers a good compromise between the number and quality of volumetric meshes. Nevertheless, the results could be improved by applying a final post-processing refinement.

Hip joint kinematics

In kinematics studies, the true hip joint center (HJC) is unknown because most techniques use external movement (motion capture data) or estimate its position relative to anatomi-

cal landmarks. In this work, the HJC is accurately computed and validated by using the reconstructed hip joint 3D model, as described in [69]. The subject movements are then recorded with an optical motion capture system (Vicon MX 13i, Oxford Metrics, UK) using 8 infrared cameras, sampling at 120 Hz. Spherical skin markers are placed on anatomical landmarks of the subject (see Figure 5A). Unlike other motion acquisition devices, the optical system allows the recording of a large range of motions that are typically used for the detection of impingements. However, the skin surface moves over the underlying structures. Rigid motion of the bone segment can therefore not be robustly estimated from the markers trajectories, unless the STA is small. Instead of trying to figure out the skin motion for each of the markers, we propose to find for each instant frame the rotation and translation that minimize the error made globally on all the markers.

During a movement, several components contribute to the motion of a skin marker. Assuming that the pelvis motion is known, the HJC can slightly move during the rotation of the thigh. This introduces one translation T_c and one rotation R. Additionally, a rigid displacement is observed due to STA which is denoted by another translation T_s. The motion of a marker with respect to the pelvis can hence be described by 3 transformations successively applied. Since an accurate estimation of both T_c and T_s is hardly possible, one of the translations must be discarded. Previous works showed that, for the thigh, the magnitude of the STA is greater that the displacement of the joint center. Therefore, we decided to compute the best estimate of T_s and to assume that T_c is close from null. Oppositely, for the pelvis, it appears that the STA remains small. Thus, for this bone we assumed that T_s is close from

null and we estimated T_c instead.

For the rotation, we choose an axis-angle representation giving us 3 values (the magnitude of the rotation is the norm of the vector). The translation gives us 3 more values, and thus 6 unknowns must be estimated from the markers motion. In order to find the transformation that minimizes the error made globally on the markers, the objective function to minimize is as follows: $\sum_n (p_i - p'_i)^2$ with n the number of markers attached to the bone segment, p_i the recorded position of the i^{th} marker, and p'_i its estimated position. This is basically a least-squares minimization for which we used the rfsqp optimizer [73].

To validate our method, a real-time dynamic MRI protocol allowing accurate bone tracking, as described in [74], was applied based on a fast gradient echo sequence. A study was carried out on 6 volunteers during an abduction motion pattern. The subjects were equipped with external MRI-compatible marker sets and a tracking device was used to ensure the movements repeatability. For each instant frame, the position and orientation of both the hip and femur bones were computed and the kinematics derived from the marker position data were compared with that of the MRI bone tracking. Table 2 shows the femur position and orientation reconstruction errors expressed in the MRI coordinates system. From these results, the errors in femur rotation are significantly reduced by the use of the proposed method with respect to the traditional one. The translation errors are a bit more significant, but are strongly related to the magnitude of STA during movements. Figure 5B shows examples of computed postures. The subject's anatomy and kinematics are taken into account and the estimation of femoroacetabular movements provides the motion input to simulate

cartilage deformation.

The simulation model

In our simulation context, we need to associate computational performance with the context of large deformations (for handling soft tissues) and high versatility (for handling collisions). Our simulation method is based on a first-order Finite-Element implementation of St-Venant-Kirchhoff materials. Full linearization of the model is not visible because of the large deformations context. Therefore, depending on the simulation context, it can be used in two modes: 1) The unrotated mode, which computes strains and stresses along predefined material axes. This approach offers the simplest and fastest computation, and allows efficient formulation of anisotropic material properties. 2) The rotated mode, which computes strains and stresses along the eigendirections of the strain tensor (corotational scheme). This approach, rather adapted to the simulation of isotropic materials, allows a more robust handling of compression (avoiding material collapse).

The elasticity strain-stress relationships are formulated using nonlinear expressions, typically modeled as polynomial splines. For anisotropic materials, six curves may be used (for the three tensile and the three shear deformation modes), complemented by additional curves using linear combinations of these six modes. This formulation offers a fairly simple, yet general modeling of nonlinear material behaviors, offering the possibility of modeling complex effects (such as volume preservation) nonlinearly. Viscosity is modeled in the same

manner, through the use of the strain rate. Plasticity results from hysteresis in the stain-stress behavior of the material. Like viscosity, the main noticeable effect of plasticity is also the material motion damping caused by energy dissipation. Our model is extended for modeling plasticity through an adequate processing of the strain-stress behavior based on Prony series approximations [75].

This model is implemented into an efficient simulation scheme which takes advantage of mass-lumping in order to get a Particle System implementation, which can support external constraints, such as those resulting from collisions, in an explicit way. A wide choice of numerical integrators can be used for relaxation or time-integration. Backward Euler is the most versatile and robust integrator, which offers quite a good performance in both of these contexts. When dynamic accuracy is more important (motion accuracy), Implicit Midpoint of 2nd-order Backward Differential Formula may also be used, at the price of robustness [76, 23]. High-accuracy dynamic simulations can also be obtained using explicit methods (Runge-Kutta) at the price of computation time. The model has been validated through comparisons with theoretical computations and commercial Finite-Element packages, demonstrating its accuracy (see Figure 6).

Results

Experimental results were obtained during the simulation of the hip joint where the articulation congruity was analyzed. The distribution of stress and strain on the deformed surface

was computed when motion was simulated. The elements present in our tests were: the hip and femur bones, as well as the femoral and acetabular cartilages reconstructed from segmented MRI data of an asymptomatic patient. The acetabular region represents the contact area. Therefore, only cartilages meshes were tetrahedralized ($\sim$20 K tetrahedra per model). A key clinical motor task in orthopaedics was then studied. It consists in applying a motion of 90° hip flexion plus a 40° internal rotation on a patient laying down. All the biomechanical materials considered in the current study were assumed as linear elastic and isotropic. The 3D models of the bones were hypothesized as rigid bodies, and the material properties for the cartilages in terms of elastic modulus (Young's modulus E) and Poisson's ratio (ν) were defined to be 12 MPa and 0.42, as depicted in [11]. While simulating the bones, collisions between the contact surfaces are automatically detected and an appropriate collision response is computed. This collision response aims constraining models to reach a non-penetrating state. Collision forces are then implemented using a penalty method [77]. Figure 7 shows a simulation example of evolving acetabular cartilage deformation during motion.

The simulation clearly demonstrates that the distribution of the strain is prone to the relevant joint angle. Deformations are mostly located in the posterosuperior region of the acetabular cartilage, which is confirmed by the clinical observations. Indeed, this is consistent with movements like flexion or abduction. During a flexion the femoral head will slide with respect to the acetabular cavity and increase stress in this region of the cartilage. This also explains why higher strain is observed in movements with high flexion and internal rota-

tion. This clinical motion is specifically used to create significant stress in the hip joint: by assessing the patient's pain tolerance, potential hip joint lesions can be detected.

Conclusion and future work

In this paper, a framework to perform functional simulations of the hip joint has been presented. This framework is composed of multiple blocks from modeling to simulation that exploit various computer graphics techniques. All these blocks were individually validated with synthetic and real trials. We have shown how these techniques yield to innovative and efficient methods in terms of speed and accuracy. The framework is applied on a simple simulation of a non pathologic joint. These first results already revealed that motion and joint structures shapes have a direct influence in the strain/ stress distribution. These are encouraging results but additional work is necessary to get a more advanced simulation.

Future work will address the following points. The complex mechanical behavior of cartilage (i.e. non-linear and biphasic properties) will be considered. A comparison study between pathological and asymptomatic patients will be computed by observing in particular the presence of abnormal stress distribution. Thanks to motion capture acquisitions, we plan to investigate more complex and extreme motion as a patient activity is undoubtedly related to the development of musculoskeletal pathologies. Finally, segmentation and tetrahedralization methods will be improved in terms of accuracy to minimize the impact of bad reconstructions in the simulation.

Acknowledgements

This work is supported by the Co-Me project funded by Swiss National Research Foundation and by the 3D Anatomical Human project funded by the European Union. We would like to thank the University Hospital of Geneva for their help and precious advice.

References

[1] Webpage Co-Me project. http://www.co-me.ch., Accessed March 2008.

[2] R. Ganz, J. Parvizi, M. Beck, M. Leunig, H. Notzli, and K. Siebenrock. Femoroacetabular impingement: a cause for osteoarthritis of the hip. *Clin Orthop*, 417:112–120, 2003.

[3] H.D. Martin. Clinical examination of the hip. *Operat Tech Orthop*, 15(3):177–181, 2005.

[4] Webpage 3D Anatomical Human project. http://3dah.miralab.unige.ch, Accessed March 2008.

[5] Y. Sato, T. Sasama, N. Sugano, K. Nakahodo, T. Nishii, K. Ozono, K. Yonenobu, T. Ochi, and S. Tamura. Intraoperative simulation and planning using a combined acetabular and femoral (caf) navigation system for total hip replacement. In *Med Image Comput and Comp Assist Intervention (MICCAI'00)*, pages 1114–1125, 2000.

[6] J. Schmitt, J. Meiforth, and M. Lengsfeld. Development of a hybrid finite element model for individual simulation of intertrochanteric osteotomies. *Med Eng Phys*, 23:529–539, 2001.

[7] E. Arbabi, R. Boulic, and D. Thalmann. A fast method for finding maximum range of motion in the hip joint. In *Comp Assist Orthop Surg (CAOS'07)*, pages 497–500, 2007.

[8] M. Kumagai, Y.H. Kim, N. Inoue, E. Genda, K. Hua B.T.L. Liong, T. Koo, and E.Y.S. Chao. 3-D dynamic hip contact pressure distribution in daily activities. In *Summer Bioeng Conf*, pages 53–54, 2003.

[9] A. Maciel, S. Sarni, R. Boulic, and D. Thalmann. Stress distribution visualization on pre- and post-operative virtual hip joint. In *Comp Assist Orthop Surg (CAOS'05)*, pages 298–301, 2005.

[10] C.C. Ahmet, U. Vahdet, and K. Recep. Three-dimensional anatomic finite element modelling of hemi-arthroplasty of human hip joint. *Trends Biomater Artif Organs*, 21:63–72, 2007.

[11] M.E. Russell, K.H. Shivanna, N.M. Grosland, and D.R. Pedersen. Cartilage contact pressure elevations in dysplastic hips: a chronic overload model. *J Orthop Surg Res*, 1(6):169–177, 2006.

[12] J. Teran, E. Sifakis, S. Blemker, V. Ng-Thow-Hing, C. Lau, and R. Fedkiw. Creating and simulating skeletal muscle from the visible human data set. *IEEE Trans Visual Comput Graph*, 11:317–328, 2005.

[13] S.S. Blemker and S.L. Delp. Three-dimensional representation of complex muscle architectures and geometries. *Ann Biomed Eng*, 33:661–673, 2005.

[14] F. Scheepers, R.E. Parent, W.E. Carlson, and S.F. May. Anatomy-based modeling of the human musculature. In *SIGGRAPH'97*, pages 163–172, 1997.

[15] T.F. Cootes, A. Hill, C.J. Taylor, and J. Haslam. The use of active shape models for locating structures in medical images. In *Int Conf Inform Process Med Imag (IPMI'93)*, pages 33–47, 1993.

[16] M.E. Leventon, W.E.L. Grimson, and O. Faugeras. Statistical shape influence in geodesic active contours. In *IEEE Conf Comput Vis Pattern Recogn (CVPR'00)*, volume 1, pages 316–323, 2000.

[17] B. Gilles, L. Moccozet, and N. Magnenat-Thalmann. Anatomical modelling of the musculoskeletal system from MRI. In *Med Image Comput Comp Assist Intervention (MICCAI'06)*, pages 289–296, 2006.

[18] T. Mcinerney and D. Terzopoulos. Deformable models in medical images analysis: a survey. *Med Image Anal*, 1(2):91–108, 1996.

[19] M. Kass, A. Witkin, and D. Terzopoulos. Snakes: Active contour models. *Int J Comput Vis*, 1(4):321–331, 1987.

[20] L. Staib and J. Duncan. Deformable fourier models for surface finding in 3D images. In *Visual Biomed Comput*, pages 90–104, 1992.

[21] H. Delingette. General object reconstruction based on simplex meshes. *Int J Comput Vis*, 32(2):111–146, 1999.

[22] A. Nealen, M. Muller, R. Keiser, E. Boxerman, and M. Carlson. Physically based deformable models in computer graphics. *Comput Graph Forum*, 25(4):809–836, 2006.

[23] P. Volino and N. Magnenat-Thalmann. Implicit midpoint integration and adaptive damping for efficient cloth simulation. *Comput Animation Virt World*, 16(3-4):163–175, 2005.

[24] Y. Wang and L.H. Staib. Physical model-based non-rigid registration incorporating statistical shape information. *Med Image Anal*, 4(1):7–20, 2000.

[25] M. Hadwiger, C. Langer, H. Scharsach, and K. Buehler. State of the art report 2004 on GPU-based segmentation. Technical report, VRVis, 2004.

[26] A.E. Lefohn, J.M. Kniss, C.D. Hansen, and T.R. Whitaker. A streaming narrow-band algorithm: interactive computation and visualization of level sets. *IEEE Trans Visual Comput Graph*, 10(4):422–433, 2004.

[27] G. Ranzuglia, P. Cignoni, F. Ganovelli, and R. Scopigno. Implementing mesh-based approaches for deformable objects on GPU. In *Eurographics Italian Chapter 2006*, pages 213–218, 2006.

[28] M.S. Shephard and M.K. Georges. Three-dimensional mesh generation by finite octree technique. *Int J Numer Meth Eng*, 32:709–749, 1991.

[29] N. Molino, R. Bridson, J. Teran, and R Fedkiw. A crystalline red green strategy for meshing highly deformable object with tetrahedra. In *Int Meshing Roundtable*, pages 103–114, 2003.

[30] R. Radovitzky and M. Ortiz. Tetrahedral mesh generation based on node insertion in crystal lattice arrangements and advancing-front delaunay tringulation. *Comput Meth Appl Mech Eng*, 187:543–569, 2000.

[31] X.Y. Li, S.H. Tang, and A. Ungor. Biting: Advancing front meets sphere packing. *Int J Numer Meth Eng*, 49:61–81, 2000.

[32] J.R. Shewchuk. Tetrahedral mesh generation by delaunay refinement. In *Annu Symp Comput Geom*, pages 86–95, 1998.

[33] S-W. Cheng and T.K. Dey. Quality meshing with weighted delaunay refinement. In *ACM-SIAM Symp. Discrete Algorithm*, pages 137–146, 2002.

[34] J.R. Shewchuk. Contrained delaunay tetrahedrizations and provably good boundary recovery. In *Int Meshing Roundtable*, pages 193–204, 2002.

[35] B. Cutler, J. Dorsey, and L. McMillan. Simplification and improvement of tetrahedral models for simulation. In *Eurographics /ACM SIGGRAPH Symp Geom Process*, pages 95–104, 2004.

[36] P. Alliez, D. Cohen-Steiner, M. Yvinec, and M. Desbrun. Variational tetrahedral meshing. In *SIGGRAPH'05*, pages 617–625, 2005.

[37] R. Schneiders. A grid-based algorithm for the generation of hexahedral element meshes. *Eng Comput*, 12:168–177, 1996.

[38] R. Schneiders. A 3d hexahedral mesh generation algorithm. engineering with computers. *Eng Comput*, 2:83–93, 1993.

[39] T.J. Tautges, T. Blacker, and S. Mitchell. The whisker-weaving algorithm: A connectivity based method for constructing all-hexahedral finite element meshes. *Int J Numer Meth Eng*, 39:3327–3349, 1996.

[40] P. Murdoch and S.E. Benzley. The spatial twist continuum. In *Int Meshing Roundtable*, pages 243–251, 1995.

[41] M.A. Price and C.G. Armstrong. Hexahedral mesh generation by medial surface subdivision. *Int J Numer Meth Eng*, 40:111–136, 1997.

[42] J. Yao and R. Taylor. Tetrahedral mesh modeling of density data for anatomical atlases and intensity-based registration. In *Med Image Comput Comp Assist Intervention (MICCAI'00)*, pages 531–540, 2000.

[43] Y. Zhang, C. Bajaj, and B-S. Sohn. Adaptive and quality 3d meshing from imaging data. In *ACM Symp Solid Model Appl*, pages 286–301, 2003.

[44] J. Crouch, S. Pizer, E. Chaney, and M. Zaider. Medially based meshing with finite element analysis of prostate deformation. In *Med Image Comput Comp Assist Intervention (MICCAI'03)*, pages 108–115, 2003.

[45] A. Cappozzo, F. Catani, A. Leardini, M.G. Benedetti, and U. Della Croce. Position and orientation in space of bones during movement: experimental artefacts. *Clin Biomech*, 11(2):90–100, 1996.

[46] D.L. Benoit, D.K. Ramsey, M. Lamontagne, L. Xu, P. Wretenberg, and P. Renstroem. Effect of skin movement artifact on knee kinematics during gait and cutting motions measured in vivo. *Gait & Posture*, 24(2):152–164, 2006.

[47] K. Manal, I. McClay, J. Richards, B. Galinat, and S. Stanhope. Knee moment profiles during walking: errors due to soft tissue movement of the shank and the influence of the reference coordinate system. *Gait & Posture*, 15:10–17, 2002.

[48] R. Stagni, S. Fantozzi, A. Cappello, and A. Leardini. Quantification of soft tissue artifact in motion analysis by combining 3d fluoroscopy and stereophotogrammetry: a study on two subjects. *Clin Biomech*, 20:320–329, 2005.

[49] A. Cappello, A. Cappozzo, P.F. La Palombara, L. Lucchetti, and A. Leardini. Multiple anatomical landmark calibration for optimal bone pose estimation. *Hum Mov Sci*, 16(2–3):259–274, 1997.

[50] L. Lucchetti, A. Cappozzo, A. Cappello, and U. Della Croce. Skin movement artefact assessment and compensation in the estimation of kneejoint kinematics. *J Biomech*, 31(11):977–984, 1998.

[51] E. Alexander and T.P. Andriacchi. Correcting for deformation in skin-based marker systems. *J Biomech*, 34:355–361, 2001.

[52] A. Cereatti, U. Della Croce, and A. Cappozzo. Reconstruction of skeletal movement using skin markers: comparative assessment of bone pose estimators. *Journal of NeuroEngineering and Rehabilitation*, 3(7), 2006.

[53] T.W. Lu and J.J. O'Connor. Bone position estimation from skin marker co-ordinates using global optimisation with joint constraints. *J Biomech*, 32:129–134, 1999.

[54] K.J Bathe. Finite element procedures. *Prentice Hall*, 1995.

[55] M. Bro-Nielsen and S. Cotin. Real-time volumetric deformable models for surgery simulation using finite elements and condensation. In *Eurographics'96*, pages 21–30, 1996.

[56] S. Cotin, H. Delingette, and N. Ayache. Real-time elastic deformations of soft tissues for surgery simulation. *IEEE Trans Visual Comput Graph*, 5(1):62–73, 1999.

[57] J. Bonet and R. Wood. Nonlinear continuum mechanics for finite element analysis. *Cambridge University Press*, 1997.

[58] M. Hauth, J. Gross, and W. Strasser. Interactive physically-based solid dynamics. In *Eurographics Symp Comput Animation*, pages 17–27, 2003.

[59] G. Picinbono, H. Delingette, and N. Ayache. Non-linear anisotropic elasticity for real-time surgery simulation. *Graph Model*, 65(5):305–321, 2003.

[60] J. Barbic and D.L. James. Real-time subspace integration for St.Venant-Kirchhoff deformable models. In *ACM Trans Graph*, 2005.

[61] M. Hauth and W. Strasser. Corotational simulation of deformable solids. In *WSCG'04*, pages 137–145, 2004.

[62] M. Muller and M. Gross. Interactive virtual materials. In *Graph Interface*, pages 239–246, 2004.

[63] G. Irving, J. Teran, and R. Fedkiw. Invertible finite elements for robust simulation of large deformation. In *Eurographics Symp Comput Animation*, pages 131–140, 2004.

[64] M. Nesme, Y. Payan, and F. Faure. Efficient, physically plausible finite elements. In *Eurographics'05*, pages 77–80, 2005.

[65] O. Etzmuss, M. Keckeisen, and W. Strasser. A fast finite element solution for cloth modeling. In *Pacific Conf Comput Graph Appl*, pages 244–251, 2003.

[66] D. Baraff and A. Witkin. Large steps in cloth simulation. In *SIGGRAPH'98*, pages 43–54, 1998.

[67] P. Volino and N. Magnenat-Thalmann. Implementing fast cloth simulation with collision response. In *Comput Graph Int 2000*, pages 257–266, 2000.

[68] M. Teschner, S. Kimmerle, B. Heidelberger, G. Zachmann, L. Raghupathi, A. Fuhrmann, M.P. Cani, F. Faure, N. Magnenat-Thalmann, W. Strasser, and P. Volino. Collision detection for deformable objects. *Comput Graph Forum*, 24(1):61–81, 2005.

[69] B. Gilles. *Anatomical and Kinematical Modelling of the Musculoskeletal System from MRI*. PhD thesis, Université de Genève, 2007.

[70] H. Blum. A transformation for extracting new descriptors of shape. In *Symp Model Percept Speech Vis Form*, pages 139–146, 1964.

[71] S.M. Pizer, P.T. Fletcher, S. Joshi, A. Thall, J.Z. Chen, Y. Fridman, D.S Fritsch, A.G. Gash, J.M Glotzer, M.R Jiroutek, C. Lu, K.E Muller, G. Tracton, P. Yushkevich, and E.l Chaney. Deformable m-reps for 3d medical image segmentation. *Int J Comput Vis*, 2(55):85–106, 2003.

[72] S. Hang. Tetgen: A quality tetrahedral mesh generator and three-dimensional delaunay triangulator.

[73] C.T. Lawrence and A.L. Tits. A computationally efficient feasible sequential quadratic programming algorithm. *SIAM J Optim*, 11(4):1092–1118, 2001.

[74] B. Gilles, R. Perrin, N. Magnenat-Thalmann, and J-P. Valle. Bones motion analysis from dynamic MRI: acquisition and tracking. *Acad Radiol*, 12:2385–2392, 2005.

[75] J.E. Soussou, F. Moavenzadeh, and M.H. Gradowczyk. Application of prony series to linear viscoelasticity. *J Rheol*, 14(4):573–584, 1970.

[76] M. Hauth and O. Etzmuss. A high performance solver for the animation of deformable objects using advanced numerical methods. In *Eurographics'01*, pages 137–151, 2001.

[77] G. Hirota, S. Fisher, A. State, C. Lee, and H. Fuchs. An implicit finite element method for elastic solids in contact. *Comput Animation*, 2001.

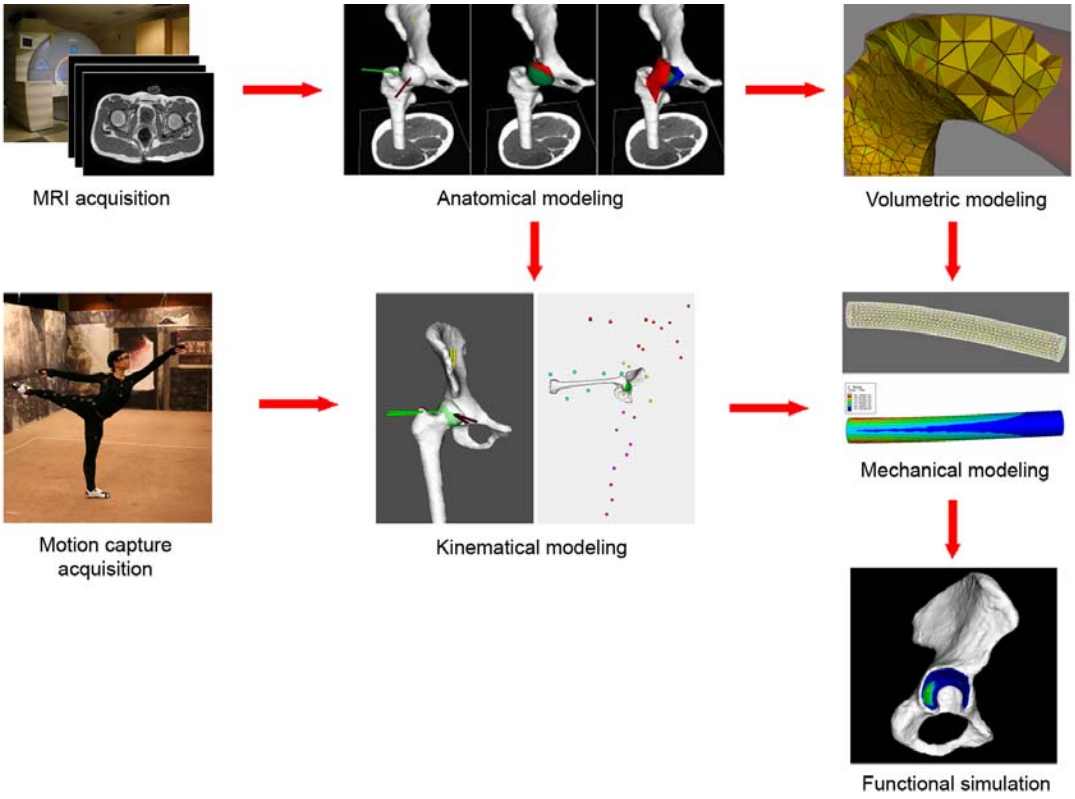

Figure 1: Overview of the methodology and workflow.

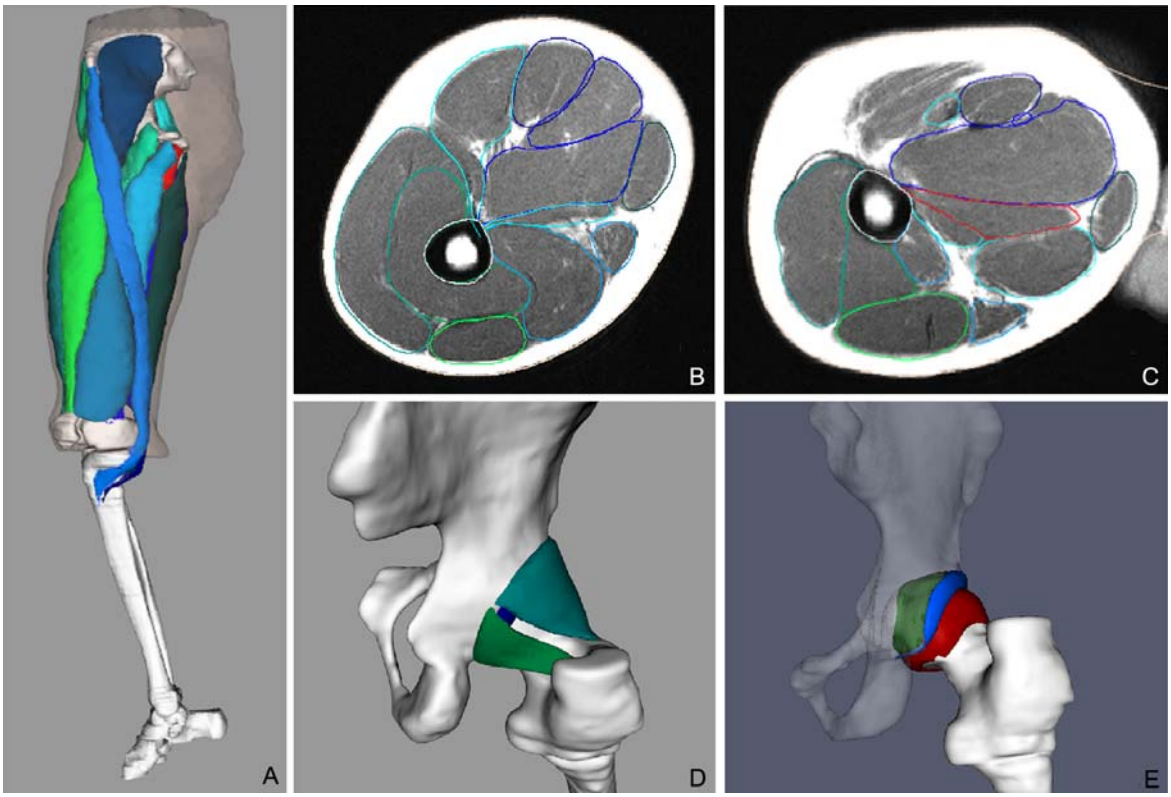

Figure 2: A) Full 3D segmented model B,C) Two MRI axial slices with segmentation overlay D) Ischiofemoral and iliofemoral ligaments E) Femoral cartilage, acetabular labrum and cartilage.

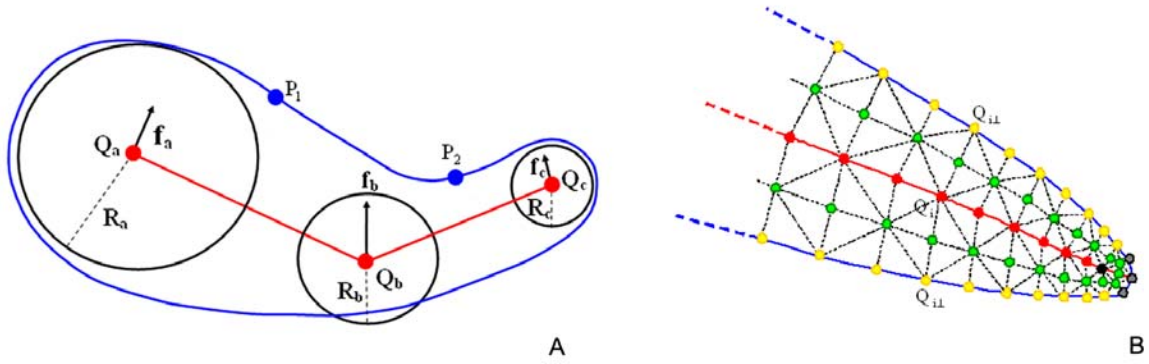

Figure 3: A) 2D example of medial axis fitting based on radial forces f_j. P_i are model points (blue), $\{Q_j, R_j\}$ are node parameters of the medial grid (red). B) 2D example of meshing: red=medial nodes, black=rim node, yellow=projected medial nodes, gray=crest nodes and green=internal nodes. Dotted lines indicated constructed cells.

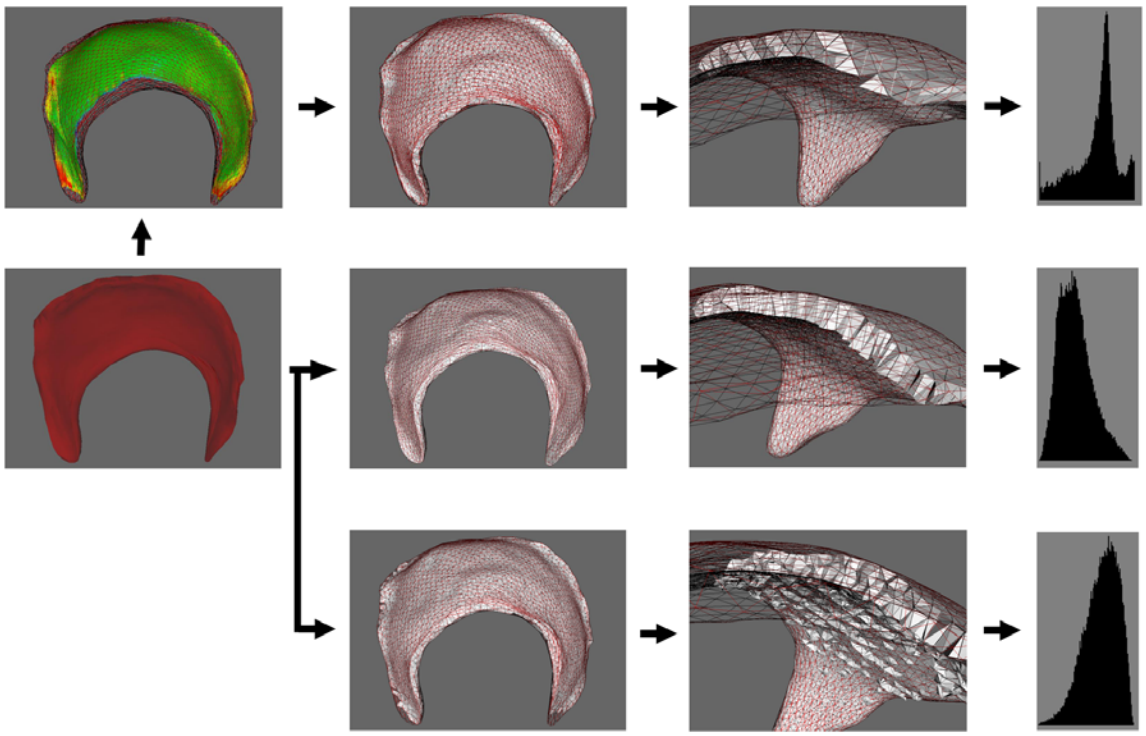

Figure 4: Comparison between tetrahedral meshes generated by the three techniques. From top to bottom: proposed approach, TetGen and VTM. From second to fourth column: entire volumetric mesh, detail of the mesh, aspect ratio histogram.

Acetabular cartilage model	Proposed approach	TetGen	VTM
Number of tetrahedra	19120	61358	61152
Av. dihedral angle [deg]	71.96	69.95	69.56
Av. aspect ratio	0.60	0.38	0.65
Envelop accuracy [mm]	0.11	0.0	0.25

Table 1: Comparison of tetrahedralization approaches. Dihedral angle: angle between tetrahedron faces, ideally 70.52; aspect ratio: three times ratio of inscribed and circumscribed spheres radius, ideally 1; envelop accuracy: root mean square of the distances between original and reconstructed surfaces.

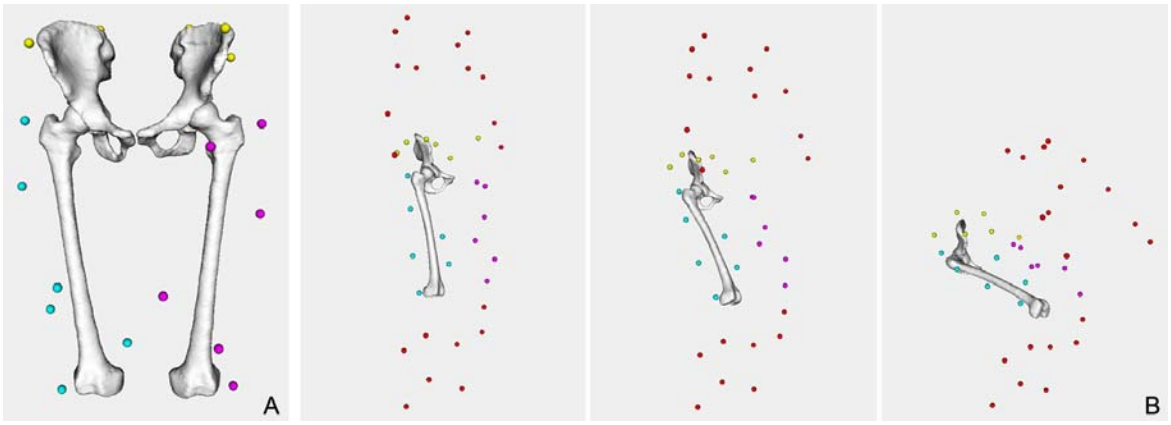

Figure 5: A) Skin markers configuration B) Examples of computed postures: stand-to-sit animation.

	X [mm]	Y [mm]	Z [mm]	α [deg]	β [deg]	γ [deg]
Mean	1.9	3.2	3.8	2.2	1.3	1.4
Root mean square	2.3	3.9	4.1	2.3	1.4	1.9
Standard deviation	1.1	2.1	1.5	0.6	0.5	1.3

Table 2: Femur position and orientation reconstruction errors.

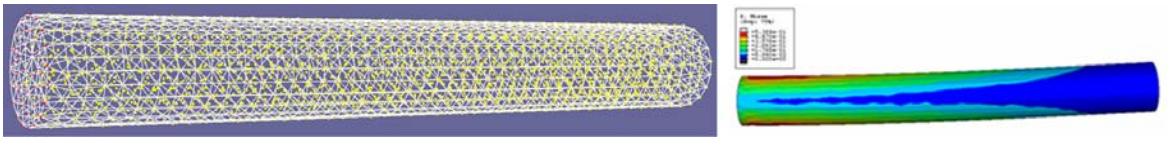

Figure 6: Validation test of our model using an elastic rod model.

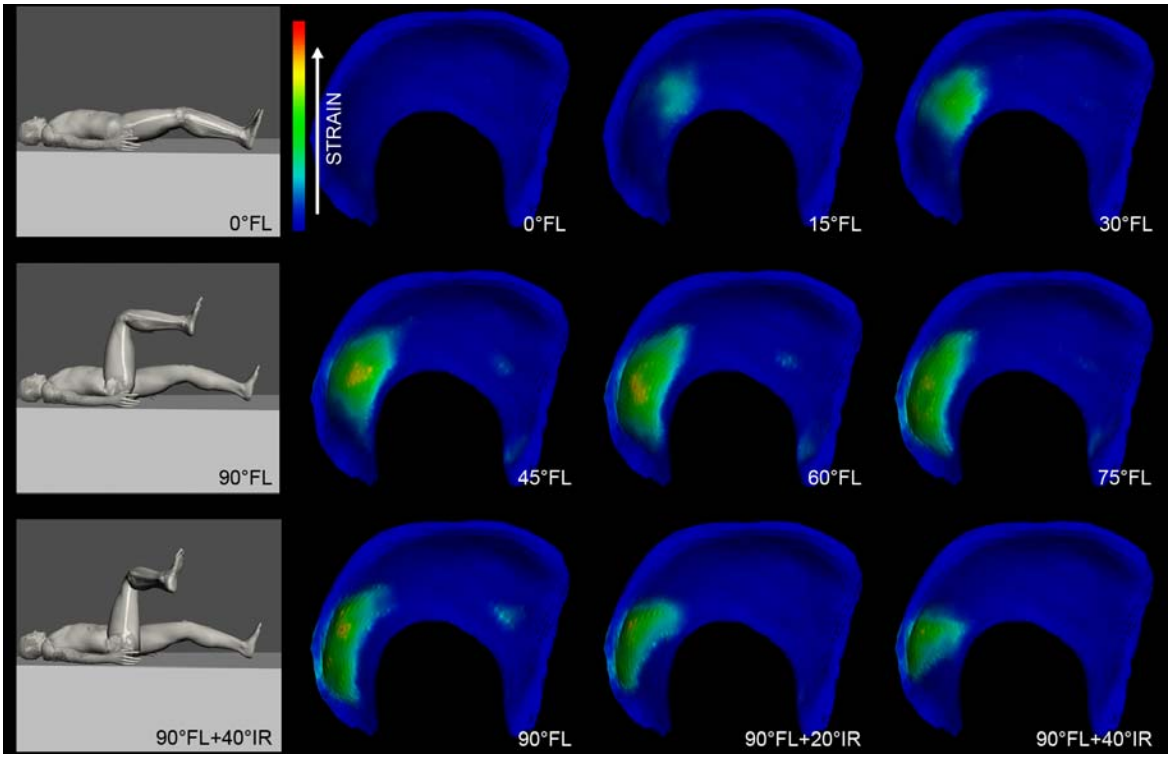

Figure 7: Average strain distribution in the acetabular cartilage during clinical motion pattern ($0° - 90°$ flexion (FL) + $0° - 40°$ internal rotation (IR)).